


# Colec12 and Trail signaling confine cranial neural crest cell trajectories and promote collective cell migration

Rebecca McLennan<sup>1,2</sup> | Rasa Giniunaite<sup>3,4,5</sup> | Katie Hildebrand<sup>6</sup> |  
 Jessica M. Teddy<sup>1</sup> | Jennifer C. Kasemeier-Kulesa<sup>1</sup> | Lizbeth Bolanos<sup>1</sup> |  
 Ruth E. Baker<sup>3</sup> | Philip K. Maini<sup>3</sup> | Paul M. Kulesa<sup>1,6</sup> 

<sup>1</sup>Stowers Institute for Medical Research, Kansas City, Missouri, USA

<sup>2</sup>Childrens Mercy Kansas City, Kansas City, Missouri, USA

<sup>3</sup>Wolfson Centre for Mathematical Biology, University of Oxford, Oxford, UK

<sup>4</sup>Faculty of Mathematics and Informatics, Vilnius University, Vilnius, Lithuania

<sup>5</sup>Faculty of Mathematics and Natural sciences, Kaunas University of Technology, Kaunas, Lithuania

<sup>6</sup>University of Kansas School of Medicine, Kansas City, Kansas, USA

## Correspondence

Paul M. Kulesa, Stowers Institute for Medical Research, Kansas City, MO 64110, USA.

Email: [pkulesa3@nd.edu](mailto:pkulesa3@nd.edu)

## Present address

Paul M. Kulesa, Department of Biological Sciences, University of Notre Dame, Notre Dame, Indiana, USA.

## Funding information

Eunice Kennedy Shriver National Institute of Child Health and Human Development, Grant/Award Number: 5R03HD089190-02

## Abstract

**Background:** Collective and discrete neural crest cell (NCC) migratory streams are crucial to vertebrate head patterning. However, the factors that confine NCC trajectories and promote collective cell migration remain unclear.

**Results:** Computational simulations predicted that confinement is required only along the initial one-third of the cranial NCC migratory pathway. This guided our study of Colec12 (Collectin-12, a transmembrane scavenger receptor C-type lectin) and Trail (tumor necrosis factor-related apoptosis-inducing ligand, CD253) which we show expressed in chick cranial NCC-free zones. NCC trajectories are confined by Colec12 or Trail protein stripes in vitro and show significant and distinct changes in cell morphology and dynamic migratory characteristics when cocultured with either protein. Gain- or loss-of-function of either factor or in combination enhanced NCC confinement or diverted cell trajectories as observed in vivo with three-dimensional confocal microscopy, respectively, resulting in disrupted collective migration.

**Conclusions:** These data provide evidence for Colec12 and Trail as novel NCC microenvironmental factors playing a role to confine cranial NCC trajectories and promote collective cell migration.

## KEYWORDS

agent-based modeling, chick, Colec12, collective cell migration, developmental biology, inhibition, neural crest, Trail

## 1 | INTRODUCTION

Vertebrate development critically relies on the long distance migration of loosely connected neural crest cells (NCCs) that are sculpted into discrete streams. After reaching peripheral targets throughout the face and neck, cranial NCCs give rise to multiple cell types including bone, cartilage, and neurons.<sup>1</sup> Failure to maintain discrete NCC migratory streams may lead to improper

anterior-to-posterior craniofacial patterning, resulting in birth defects termed neurocristopathies.<sup>2,3</sup> Repair of neurocristopathies may result in significant costs associated with successive corrective surgeries.<sup>4,5</sup> Thus, a better understanding of the mechanisms that underlie the confinement of cranial NCC trajectories and promotion of collective cell migration would provide insights into the root causes of neurocristopathies and inform emerging stem cell-based tissue repair strategies.<sup>6</sup>

Despite the discovery of chemical signals that attract NCCs toward peripheral targets,<sup>7-10</sup> several unanswered questions remain. In this paper, we address the following questions: (a) what are the signals that confine cranial NCC trajectories to stereotypical migratory pathways; and (b) how do these signals promote collective NCC migration? In the head, cranial NCCs emerge all along the vertebrate axis of the hindbrain and are sculpted to exit into the paraxial mesoderm adjacent to even-numbered rhombomeres (denoted by *r*). The tissue origins and molecular components of the signals within the hindbrain that regulate cranial NCC behaviors immediately after dorsal neural tube exit have been well-studied (reviewed by Trainor and colleagues<sup>11-13</sup>). For example, repulsive signals present in the dorsal neural tube microenvironment during *r3* neuroepithelium and *r3* surface ectoderm interactions prevent cranial NCCs from turning anterior or posterior shortly after exiting from the midline of either *r2* or *r4*, through *ErbB4* receptor and neuregulin ligand interactions.<sup>14</sup> After NCCs exit into the paraxial mesoderm, disruption of semaphorin-neuropilin signaling either by overexpression of soluble Neuropilin-1/2 Fc in chick<sup>15</sup> or in mice carrying null mutations for either Neuropilin-2 or its ligand *Sema3F*<sup>16</sup> results in diversion of *r4* NCCs away from the stereotypical migratory pathway. This loss of NCC confinement immediately adjacent to the neural tube (within 0–200  $\mu\text{m}$  from the dorsal midline) results in the formation of narrow, single cell-wide cellular bridges between the *r2* and *r4* NCC migratory streams. Together, these signals prevent uncontrolled NCC invasion shortly after neural tube exit and suggest the presence of other inhibitory signals further away from the influence of the dorsal hindbrain that confine NCC trajectories.

Signals that confine cranial NCC trajectories near the target branchial arches 1-4 (*ba1-4*) are well-studied. Complementary expression of *EphA4/EphB1* receptors and Ephrin-B2 ligand on migrating *Xenopus* cranial NCCs restricts intermingling of closely juxtaposed *r4* and *r6* streams to ensure proper invasion into *ba2* and *ba3*, respectively.<sup>17</sup> More recently, *Versican* has been reported to confine *Xenopus* cranial NCC migration. However, its knockdown by morpholino reveals that migrating NCCs do not undergo widespread intermingling between neighboring streams as expected, complicating its role as a permissive or inhibitory factor.<sup>18</sup> Moreover, *Versican* expression is present in *Xenopus* placodal tissues near the branchial arches, suggesting a later role to prevent NCC stream mixing prior to branchial arch entry.<sup>18</sup> In the chick, examination of Eph/ephrin expression in cranial NCC streams that are more widely separated by NCC-free zones revealed *EphA3*, *EphA7*, and *EphB3* expression in migrating *r4* cranial NCCs.<sup>19</sup> Although *EphB2* and

Ephrin-B1 confine migrating chick cranial NCCs in protein stripe assays, their *in vivo* expression in the mesoderm lateral to the otic vesicle (*EphB2*) and within the target *ba2* (Ephrin-B1) make these factors unlikely candidates to confine *in vivo* cranial NCC trajectories between the dorsal neural tube and branchial arch entrances. Thus, the identification of microenvironmental factors along the cranial NCC migratory pathways and their function in regulating dynamic *in vivo* cell behaviors to promote collective migration remain unclear.

Computational models are well-equipped to investigate the role of confining signals in collective cell migration. Szabo et al<sup>18</sup> used agent-based modeling in the context of tightly coupled *Xenopus* NCC clusters to predict that the optimal two-dimensional (2D) confinement width (coinciding with the anteroposterior length along the axis from which cells emigrate) is proportional to the number of migrating cells. From this work, a more detailed mechanochemical model of *Xenopus* NCC cluster migration integrating cell polarity signaling through Rac1 and RhoA,<sup>20,21</sup> confirmed these predictions. Szabo et al<sup>22</sup> then integrated their data on *Versican* expression to simulate the interaction between migrating NCC clusters with distally located placodal cells. They interpreted their experimental results and model simulations to speculate that confinement of NCC trajectories promoted collective cell migration by keeping cells close to each other, allowing for proper functioning of contact inhibition of locomotion (CIL)/Co-attraction (Co-A).<sup>23</sup> However, the width of this corridor must be optimized since the CIL/Co-A mechanism breaks down when cells are confined to a narrow corridor.<sup>21</sup>

In contrast to modeling the migration of tightly clustered NCCs, agent-based models of loosely connected NCC streams have elucidated the leader-follower mechanism of collective cell migration; leader cells readout guidance signals and communicate them to follower cells.<sup>24,25</sup> The discovery of the BMP-antagonist Dan (Differential Screening-Selected Gene Aberrant in Neuroblastoma) present in the chick paraxial mesoderm and *in vitro* confinement of cranial NCCs in stripe assays posed the question of its *in vivo* function.<sup>26</sup> By using this modeling framework that relaxed the previous 2D reflecting boundary conditions present in both leader-follower<sup>24,25</sup> and CIL/Co-A<sup>23</sup> models and replaced them with a Dan-region, simulations showed that slowing leader cell migration through the Dan-region resulted in robust collective cell migration.<sup>27</sup> Thus, computational modeling frameworks offer a powerful and rapid approach to determine the mechanisms and parameters of cell confinement and collective cell migration and are, therefore, well-placed to guide experimental investigation.

In this study, we integrated computational modeling and experiments to study the requirements of spatial confinement of NCC trajectories and how this confinement promotes collective cell migration. Model simulations focused on determining the minimum requirements of a “spatial confinement boundary” along the anterior and posterior borders of a 3D migratory domain extending in the distal direction away from the neural tube and to maintain a discrete NCC stream over long distances. This helped to direct experimental analyses of previously undescribed factors in the embryonic NCC microenvironment as Colec12 (Collectin-12 [or CL-12], a transmembrane scavenger receptor C-type lectin<sup>28</sup>) and Trail (tumor necrosis factor-related apoptosis-inducing ligand, CD253<sup>29</sup>), part of a subset of genes we identified by profiling chick cranial mesoderm.<sup>26</sup> By using our integrated RNAscope fluorescence in situ hybridization (FISH), immunohistochemistry, and tissue clearing method,<sup>30</sup> we analyzed the 3D expression patterns of Colec12 and Trail with respect to migrating cranial NCCs in the intact chick embryo. Protein stripe assays and coculture in the presence of either Colec12 or Trail protein allowed us to evaluate the confinement of cranial NCC trajectories and dynamic changes in cell morphology and migratory characteristics. After in vivo gain- or loss-of-function of single or multiple combinations of these factors, we measured the extent of NCC diversion away from stereotypical migratory streams and into typical NCC-free zones, using confocal time-lapse imaging to visualize changes in cell behaviors. Together, our results predict the spatial requirements to confine cranial NCC trajectories to discrete streams, characterize Colec12 and Trail expression as consistent in space and time with computer model predictions, and demonstrate their functional roles to confine NCC trajectories and promote collective cell migration.

## 2 | RESULTS

In our previous work, we focused our computational modeling of cranial NCC migration solely on the corridor connecting r4 to ba2 with boundary conditions adjacent to (rostral and caudal borders) along the entire length (proximal-to-distal) of the migration corridor to ensure that cells stay confined to the corridor (Figure 1). Here, we relax this assumption and, instead consider the larger domain that also includes the nearest neighboring corridors emanating adjacent to r3 and r5. In this case, the corridor of interest (r4 to ba2) is now a subset of this larger domain (Figure 1A). Within this larger domain, we will consider internal boundary conditions that confine cells to the corridor of interest by imposing zero flux

boundary conditions along part of the r4-ba2 corridor (Figure 1A). We refer to such cases as an internal confinement boundary.

### 2.1 | Model simulations predict the full length of an internal confinement boundary is *not* required to maintain discrete streams over long distances

We use our computational model to explore the effects of spatial confinement on the cranial NCC migratory pattern. The model is of hybrid off-lattice (agent-based) type, in which cells are agents whose motility is coupled to a continuum, reaction-diffusion model of the dynamics of the known cranial NCC chemoattractant vascular endothelial growth factor (VEGF)<sup>7</sup> on a growing rectangular 2D domain (described in Section 4). In the model, cells adopt one of two possible phenotypes, leader or follower, and here we specify a fixed number of leader cells. The cells may change their phenotypes based on their position within the migratory stream (see Section 4). Leader cells sample the microenvironment through the extension of three filopodia and move in the direction of the highest concentration of chemoattractant sensed, provided it is higher by a threshold value than that at the position of the center of the cell (the cell moves randomly if there is no measured difference). If follower cells are in a stream, defined as a group of cells that are close to each other with at least one of the cells a leader, they move in the same direction as the leader cell in that stream. If follower cells are in a tunnel, they move along the tunnel defined as a directed path created by a leader cell. If follower cells are not in a stream or tunnel, the cells move randomly.

In simulations of the full length of an internal confinement boundary with follower cells guided by stream and/or tunnels, we find cells reach the target without a breakdown of collective cell migration (i.e., the majority of follower cells are in streams and/or tunnels; Figure 1A). In contrast, without an internal confinement boundary, cells may migrate away from the stereotypical pathway, resulting in a considerable breakdown of collective migration (Figure 1B). To compare the migratory patterns of cells in the model for increasing the extent of an internal confinement boundary (Figure 1C), we quantified two different stream characteristics. We first consider the likelihood of a breakdown of collective migration, defined as the fraction of cells not in streams or tunnels at the end of a simulation (Figure 1D,E). We determined that breakdown of collective migration is most likely when the internal confinement is short (0–200  $\mu\text{m}$ ) in both model scenarios: (a) When follower cells

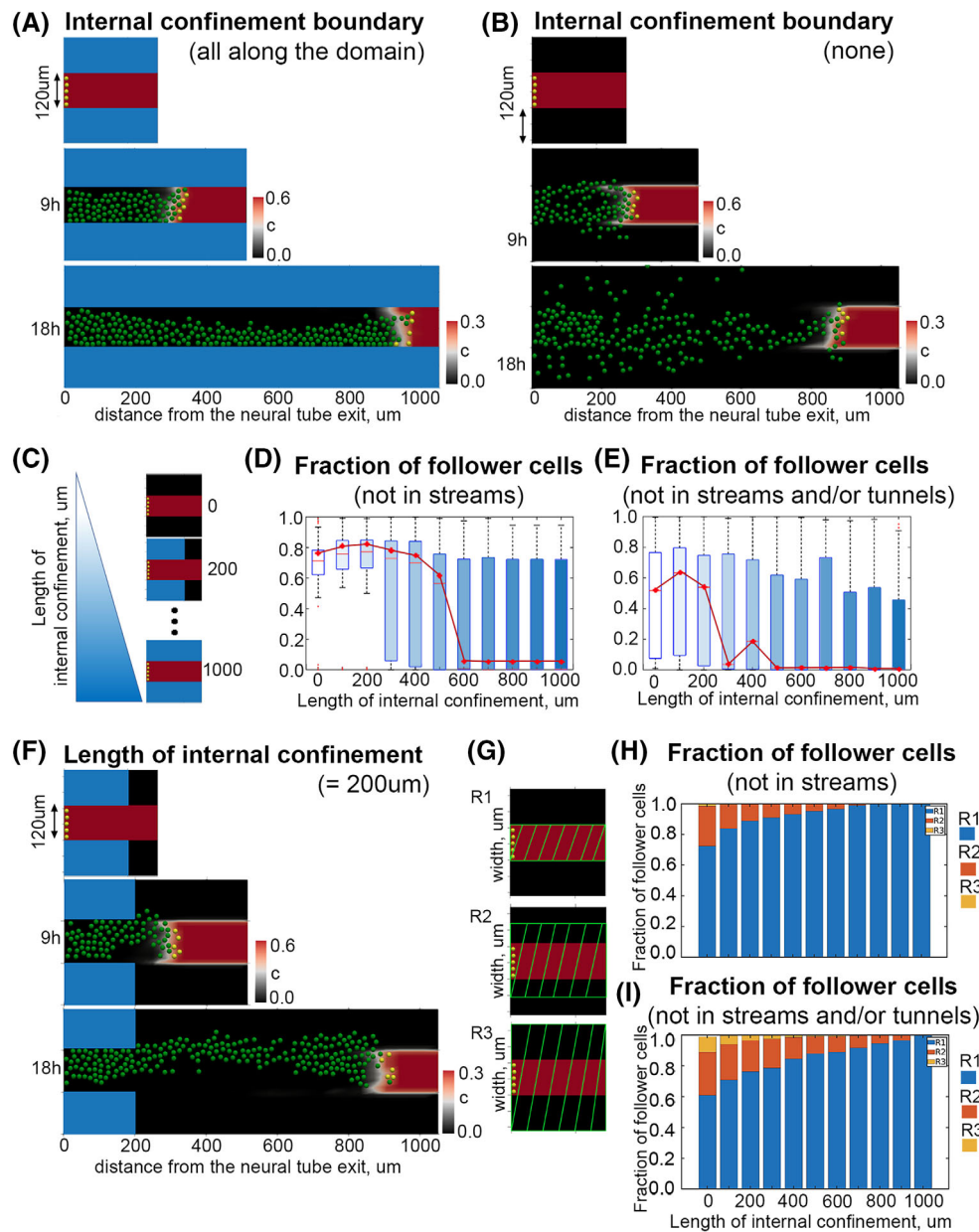


**FIGURE 1** Computer model simulations predict that neural crest cell confinement along the entire length of the migratory domain is not required to maintain discrete neural crest cell (NCC) streams over long distances. Different confinement possibilities for the initial set up: (A) full internal confinement; (B) no internal confinement. The red rectangle corresponds to the region with uniform initial chemoattractant concentration,  $c = 1$ . The chemoattractant concentration in the black region is zero,  $c = 0$ . The blue rectangles represent internal confinement subregions adjacent to rhombomeres 3 (r3) and r5. Yellow circles represent NCCs. C, Shades of blue corresponding to different extents of internal confinement. D, Boxplots of fractions of follower cells not in streams and/or tunnels (E) at  $t = 18$  h. This statistic corresponds to the likelihood of breakdown of collective migration. For each model, the red line indicates the median, and the bottom and top edges of the boxes indicate the 25th and 75th percentiles, respectively. The dotted lines extend to the most extreme data points not considered outliers, and the outliers are plotted individually as red dots. The breakdown of collective migration is most likely when there is a short internal confinement length. For the same internal confinement length, the stream is less likely to break for streams/tunnels model (right) than for streams only model (left). One thousand twenty micrometers corresponds to a full internal confinement boundary. F, Partial (200  $\mu\text{m}$ ) internal confinement. G, Different subregions (indicated by the green diagonal lines) that are used to quantify how widely the cells are spread out. H, Fraction of cells in different subregions (1, 2, or 3) for the model scenario of streams and/or tunnels (I). In (D), (E), (H), (I) results are averaged over 100 simulations.

may only form streams (Figure 1C,D); (b) When cells can form streams and move through leader-created tunnels (Figure 1C,E). This result is to be expected because when

the cells are free to travel in an unrestricted wide region, it is more difficult for them to find streams or tunnels, resulting in breakdown of collective migration. The

likelihood of breakdown of collective migration decreases as the extent of an internal confinement boundary is increased, again, as expected (Figure 1C–E). Unexpectedly, the model predicts that even with a relatively short spatial confinement length of 0–600  $\mu\text{m}$  (Figure 1D; streams) or 0–500  $\mu\text{m}$  (Figure 1E; stream and/or tunnels) the likelihood of breakdown in collective migration is low (i.e., efficient collective cell migration), implying the critical importance of an internal confinement boundary as cells exit the neural tube and start the first phase of migration (Figure 1D–F). The average likelihood of breakdown in collective migration is almost zero for an internal confinement boundary of length greater than or equal to 600  $\mu\text{m}$  (Figure 1D,E). We conclude that the cell confinement along the entire length of the migratory domain is not necessary to avoid breakdown in collective migration. To this end, biological inhibitory signals are only required in the approximately first one-third of the migratory domain.

We also investigated to what extent the cells spread out in the  $y$ -direction when different lengths of an internal confinement boundary are considered (Figure 1G–I). To this end, we defined three subregions, recorded the  $y$ -coordinate of each cell at the end of a simulation and calculated the fractions of cells in different subregions. Subregion 1 corresponds to the observed NCC migratory domain (width—120  $\mu\text{m}$ , Figure 1G; R1). Subregion 2 corresponds to a weak deviation from the biologically realistic migratory domain (width—240  $\mu\text{m}$ , Figure 1G; R2); subregion 3 corresponds to a large deviation from the biologically realistic NCC migratory domain (width—360  $\mu\text{m}$ , Figure 1G; R3). We find that there is a monotonic decrease in the fractions of cells in subregions 2 and 3 when the length of the internal confinement is increased in both model scenarios (Figure 1H,I). Taken together, simulations of our model, which considers chemotactic cell movement and various cell-cell interactions with varying levels of cell confinement, demonstrate that unknown inhibitory signals within the neural crest microenvironment play a crucial role in the collective migration of NCCs from neural tube exit through approximately the first one-third of the stereotypical r4 migratory pathway.

## 2.2 | Colec12 and Trail are present in the chick cranial mesoderm and show restricted expression within cranial NCC-free zones

COLEC12 has been characterized in vascular endothelial cells and its knockdown in zebrafish causes severe defects in vasculogenesis and development.<sup>31</sup> TRAIL and its

receptors, TRAIL-R1 and TRAIL-R2, selectively trigger apoptotic cell death in tumor cells and has been extensively studied as a target of cancer treatment.<sup>32,33</sup> However, the expression of both factors has not been examined in the embryonic NCC microenvironment and there is no known functional role for either factor in collective cell migration.

To first determine the mRNA expression patterns of *Colec12* and *Trail* with respect to migrating cranial NCC positions, we performed a detailed analysis across chick developmental stages corresponding to NCC exit from the neural tube throughout migration to the branchial arches (stages HH11, HH13, and HH15; using Hamburger and Hamilton<sup>34</sup>). Using multiplexed FISH on whole (HH11) or half mount embryo heads (HH13 and HH15), we determined that both *Colec12* and *Trail* expression is enhanced within the presumptive NCC-free zone adjacent to r3 (Figure 2A,B). Specifically, we find that the rostral and caudal borders of *Colec12* expression at HH11–13 within the tissue adjacent to r3 are juxtaposed to the r1–r2 and r4 NCC migratory streams marked by *Sox10* expression (Figure 2A). *Trail* expression in the subregion adjacent to r3 is slightly diffuse in comparison to *Colec12* (Figure 2B) with *Sox10* expression marking the migrating NCCs (Figure 2B, open circle). Transverse sections through the hindbrain clearly show that *Colec12* mRNA is present in the mesoderm adjacent to the neural tube and extending to approximately 400  $\mu\text{m}$  away from the neural tube (Figure 2C).

## 2.3 | Cranial NCCs avoid Colec12 and Trail protein in vitro stripe assays

To test whether NCCs avoid *Colec12* and/or *Trail* protein in culture, we explanted cranial neural tubes onto stripe assays and performed both static and time-lapse analyses (Figure 2D–F). Static analysis of NCC positions after 12 h of incubation on the stripe assays showed a dramatic difference in the number of cells on either *Colec12*-, or *Trail*-containing stripes (Figure 2D,E). Migrating NCCs mostly avoided *Colec12*- or *Trail*-containing stripes; only around 25% of migrating NCCs were found on these protein stripes, in comparison to the negative control that showed a nearly equal distribution of migrating NCCs on and off stripes (Figure 2D,E). Time-lapse imaging of dynamic NCC behaviors revealed distinct responses depending on the presence of either *Colec12* or *Trail* protein (Figure 2E). Specifically, when exposed to *Colec12* stripes, the initial NCCs to delaminate from the neural tube avoided the *Colec12*-positive stripes and appeared to form discrete streams (Figure S1B; see Movie S1). Some NCCs that exited onto the *Colec12*-positive stripes rapidly

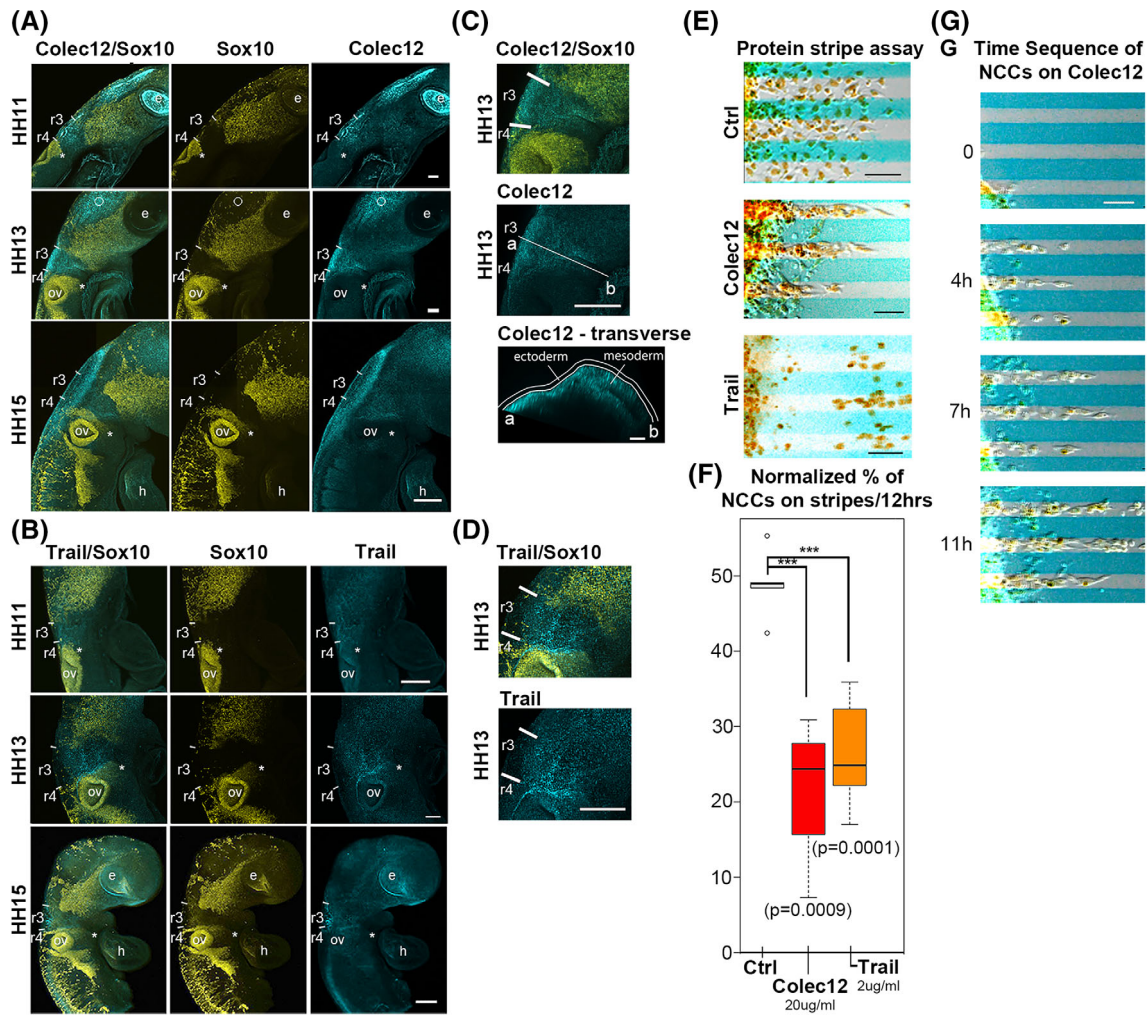


**FIGURE 2** Colec12 and Trail expression are enhanced in neural crest cell free zones and confine neural crest cell trajectories in protein stripe assays. **A**, Colec12 expression (light blue) in the chick head at HH11, HH13, and HH15 with Sox10 (gold) marking the migrating NCCs; the migratory front of the r4 stream is marked by an asterisk. The rhombomeres r3 and r4 are labeled with short white lines marking the rhombomere boundaries in the neural tube. Colec12 expression is also in the region rostral to r1 and adjacent to the midbrain (marked by an open circle at HH13). **B**, Trail expression (light blue) in the chick head at HH11, HH13, and HH15 adjacent to r3 with Sox10 (gold) marking the migrating NCCs; migratory front of the r4 stream marked by an asterisk. The rhombomeres r3 and r4 are labeled with short white lines marking the rhombomere boundaries in the neural tube. **C**, Same embryo image as in (A; HH13) with individual images of Colec12 staining. The line marked a to b is the plane of the yz image collected. **D**, Same embryo image as in (B; HH13) with individual images of Trail staining. **E**, Typical protein stripe assays show confinement of NCCs with Ctrl, Colec12, and Trail on the protein stripes (light blue) vs. fibronectin only in the control. **F**, Boxplot graph of the normalized percentage of NCCs on stripes. **G**, Sequence of images from a typical time-lapse imaging session show the cranial neural tube explant (left) and migrating NCCs confined to the lanes without Colec12 protein (light blue). In (A, B), the eye (e), otic vesicle (ov), and heart (h) are labeled where appropriate. The scalebars in (A) are 50  $\mu\text{m}$ , in (B) are 100  $\mu\text{m}$  (HH11), 50  $\mu\text{m}$  (HH13), and 100  $\mu\text{m}$  (HH15), in (C–F) are 50  $\mu\text{m}$ .

reversed direction back toward the explanted neural tube (Figure S1C). As NCCs moved within the corridors between the Colec12-positive stripes, cells were observed to move onto Colec12-positive stripes, but did so in a rapid manner to cross to a neighboring stream of NCCs on a Colec12-negative stripe (Figure S1D; see Movie S1). In contrast, when cranial neural tubes were explanted onto Trail protein stripes, we observed the delaminating NCCs retract cell protrusions. NCCs that did delaminate

successfully from the explanted neural tubes crowded onto the control stripes in clusters and immediately avoided the Trail-positive stripes (Figure 2D). Any individual NCCs observed on the Trail-positive stripes migrated perpendicular to the stripes and onto the control stripes (data not shown). These data clearly demonstrate that either Colec12 or Trail protein may confine NCC trajectories, with distinct cell behaviors in response to the protein stripes.

## 2.4 | Colec12 or Trail protein introduced onto the NCC migratory pathway enhanced confinement of cell trajectories

To begin to test the *in vivo* effects of perturbing Colec12 and Trail signaling on cranial NCC migration, we overexpressed these factors by microinjection of the same human recombinant proteins as used in the stripe assays. Microinjections were directed into the paraxial mesoderm adjacent to r4, prior to NCC emigration from the dorsal neural tube (Figure 3). After 16 h of egg reincubation, we harvested embryos and compared the NCC migration pattern on injected vs. non-injected (control) sides, using HNK1 to fluorescently mark migrating NCCs (Figure 3A–D). Introduction of either Colec12 or Trail led to enhanced confinement of NCC streams, as measured by the reduction in area covered by the typical migratory stream in comparison to the non-injected side of the

embryo (Figure 3E). Control PBS injections saw no significant changes (Figure 3E). Combined microinjection of both Colec12 and Trail simultaneously into the r4 paraxial mesoderm led to a stronger phenotype of reduced cranial NCC confinement (Figure 3E). These results show that introduction of Colec12 and/or Trail protein directly onto the cranial NCC migratory pathway prior to NCC emigration can significantly enhance the confinement of *in vivo* NCC trajectories.

## 2.5 | Knockdown of Colec12 leads to precocious invasion of cells into the presumptive NCC-free zones and disruption of collective cell migration

To determine whether blocking of Colec12 signaling would result in NCC invasion into typical NCC-free

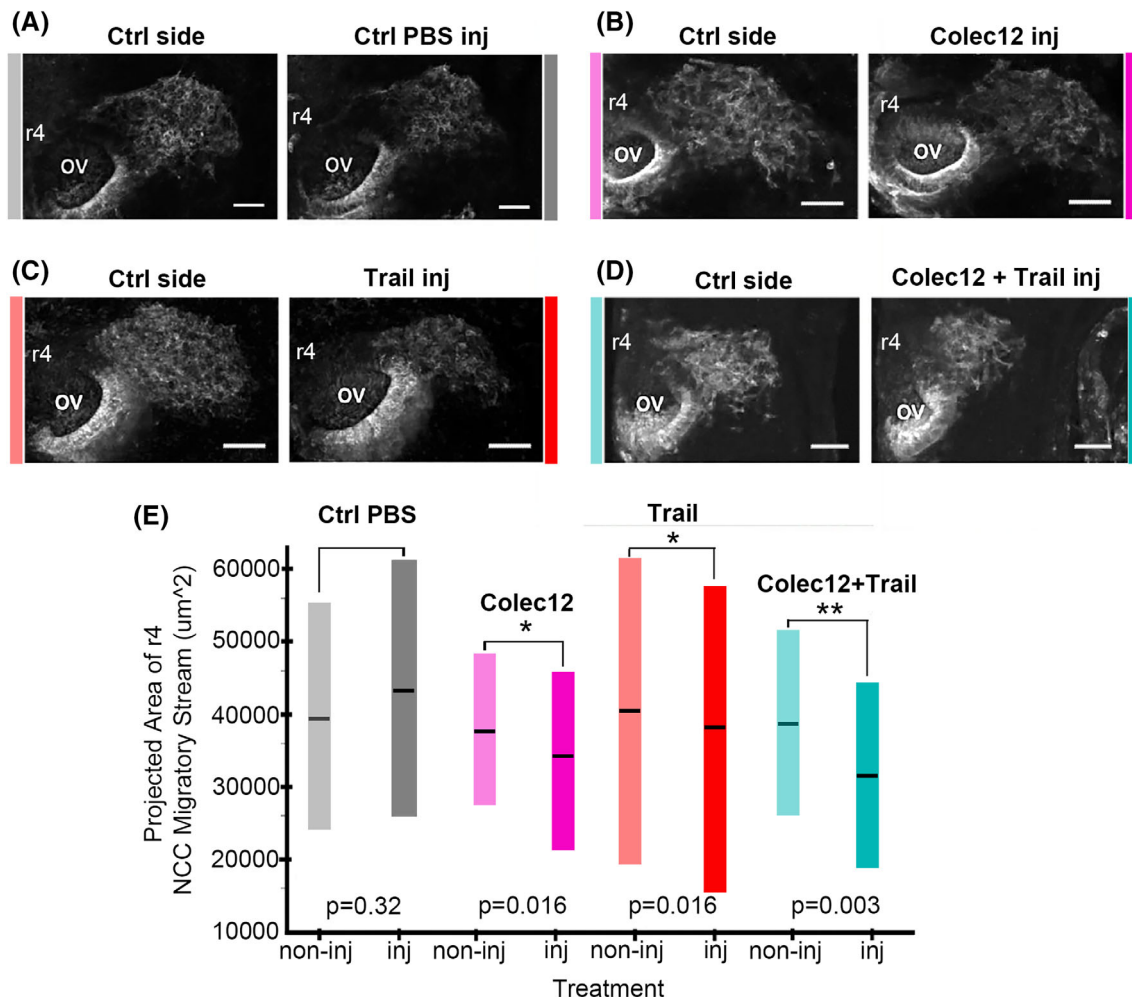


**FIGURE 3** Microinjection of Colec12 or Trail protein or in combination onto the presumptive r4 NCC pathway enhances confinement of NCCs. A, Control (Ctrl) PBS injection into the right-hand side of the chick embryo and control non-injected side (left) showing the r4 NCC migratory stream and otic vesicle (ov). B, Colec12. C, Trail. D, Colec12 + Trail. E, Measurement of the projected area of coverage of the r4 NCC migratory stream in each of the control and perturbation scenarios. The scalebars are 50 μm in all images.

zones, a translation-blocking morpholino was used to reduce the expression of *Colec12* in the typical NCC-free zone adjacent to r3. After 24 h of egg reincubation and embryo harvesting, we observed significant changes to migrating NCC morphologies adjacent to the NCC-free zone, increased numbers of migrating NCCs within the mesoderm lateral to r3, and an increased area of NCC migratory streams when compared to control sides in the same embryo or embryos transfected with a control morpholino (Figure 4A–F). NCCs along the rostral border of the r4 NCC migratory stream had distinct cell protrusions toward the subregion lateral to r3 and a disruption in cell morphologies was observed in *Colec12* MO injected vs. control MO embryos (Figure 4A–D, insets). To quantify this phenotype during mid-migration of NCCs from the neural tube to the end of the branchial arches, we performed the same experiment but reincubated eggs for 12 h only. We found that the number of NCCs that invaded the typical r3 NCC-free zone was significantly higher when compared to control sides of the same embryo or embryos transfected with a control morpholino (Figure 4E). Moreover, there was a significant difference in the typical area covered by the r4 NCC migratory stream in *Colec12* MO embryos, reducing collective cell migration over long distances (Figure 4F).

In order to thoroughly investigate the dynamic responses of cranial NCCs to the inhibitory nature of *Colec12* in vivo, we transfected mesodermal cells with *Colec12* morpholino or control morpholino and performed time-lapse confocal imaging of intact chick embryos. When endogenous *Colec12* was knocked down in the typical r3 NCC-free zone, we observed two unique phenomena. First, the r4 NCC migratory stream widened toward the r3 NCC-free zone—this was not observed on the control side (Figure 4G, first frame of sequence at  $t = 0$ ). Second, in a typical time-lapse imaging session we observed a secondary stream of NCCs (Figure 4G, arrow at  $t = 2$  h) that diverted from the r4 NCC migratory stream (Figure 4G, asterisk) and continued to invade into the r3 NCC-free zone (Figure 4G, arrow at  $t = 4$  h). Together, these data clearly demonstrate an in vivo role for *Colec12* in confining cranial NCCs to the stereotypical r4 migratory pathway and promoting collective cell migration.

## 2.6 | Combined knockdown of *Colec12* and *Trail* enhanced invasion of NCCs into the presumptive NCC-free zones and further disrupted collective cell migration

In humans, TRAIL has five known receptors, including the death receptor 4 (DR4), DR5, decoy receptor 1 (DR1),

DR2, and osteoprotegerin<sup>35–38</sup> and of these, the avian system has two homologs. *Tnfrsf10b* and *Tnfrsf11b* are the avian homologs of the human genes of the same names; *Tnfrsf10b* contains a cytoplasmic death domain, while *Tnfrsf11b* is a secreted decoy receptor. Both of these receptors are expressed by migrating r4 cranial NCCs at the RNA level.<sup>39</sup> To inhibit cranial NCC interactions with Trail, we transfected premigratory NCCs with morpholinos designed against *Tnfrsf10B* and *Tnfrsf11B*. When either *Tnfrsf10b* only or both receptors are knocked down and embryos harvested and analyzed after 12 h, we find invasion of NCCs into the typical r3 NCC-free zones (Figure 4H,J). We then focused on inhibiting both *Colec12* and Trail proteins by microinjection and transfection of the *Colec12* morpholino directly into the mesoderm adjacent to r3 and either *Tnfrsf10B* morpholino only or both *Trail* receptor morpholinos into premigratory NCCs. When both *Colec12* and Trail signaling were inhibited, we observed a significant increase in the number of migrating NCCs and extensive invasion of the r3 NCC-free zone at both 12 and 24 h after embryo harvesting and imaging (Figure 4I,K). Specifically, both individual cells and NCC streams diverted from the r4 migratory stream and invaded the r3 NCC-free zone; with a more striking phenotype at the 12 h time point (Figure 4I,K). These data strongly support the roles of *Colec12* and Trail in confining cranial NCC trajectories and signaling through mutually exclusive pathways to promote collective cell migration.

## 2.7 | Cranial NCCs exposed to *Colec12*, or Trail protein in the culture media show significant and distinct changes in cell morphology and dynamic migratory characteristics

To better understand the function of *Colec12* and Trail in influencing NCC migratory behaviors and to promote collective cell migration, we plated isolated cranial neural tubes in the presence of *Colec12* or Trail protein added directly into the culture media (Figure 5A). Changes in cell morphology and cell behaviors were visualized using time-lapse confocal imaging and quantified (Figure 5B–E). We find that NCCs cultured in the presence of *Colec12* protein exhibited persistent, lengthened protrusions with increased branching (Figure 5B; compare Ctrl vs. +*Colec12* images; compare Movies S2 and S3). When individual NCCs were closely observed in the presence of *Colec12* protein, we noticed that the tips of each extended filopodium appeared unable to retract (see Movie S3). Static measurements after 8 h in culture confirmed significantly longer filopodial extensions (Figure 5E); cell speed



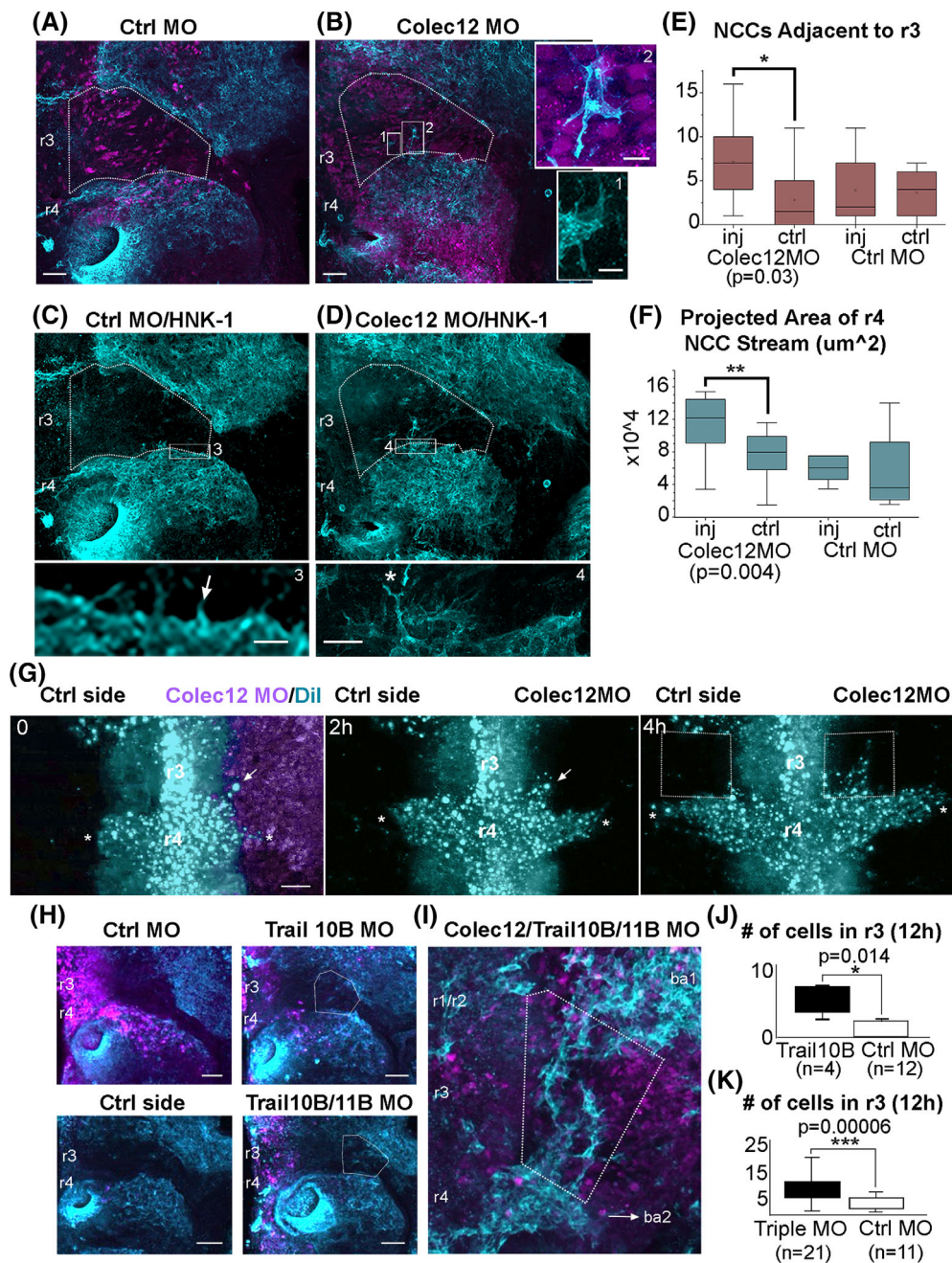


**FIGURE 4** Knockdown of Colec12 and/or Trail leads to diversion of NCCs into the presumptive NCC-free zones. (A) Control (Ctrl) and (B) Colec12 morpholino (MO) in purple showing the migrating NCCs (HNK1; blue). The subregion adjacent to r3 (typical NCC-free zone) is enclosed by a dotted line. In the Colec12 MO image, note the diversion of NCCs into this subregion with individual diverted NCCs (boxed, 1 and 2; insets). C, D, HNK-1 staining only of the (C) Ctrl MO and (D) Colec12 MO. Note the differences in the rostral border of the r4 NCC migratory stream (boxed, 3 and 4; insets) showing the short NCC protrusions and coherent border (box 3; arrow) in contrast to lengthy NCC protrusions and disrupted border (box 4; asterisk). E, F, Measurements of the number of diverted NCCs into the subregion adjacent to r3 and projected area of the r4 NCC migratory stream in control vs. Colec12 morpholino embryos ( $n = 12$  embryos in each experiment). G, Sequence of images (0, 2, 4 h) from a typical time-lapse imaging session with DiI-labeling of NCCs (blue) showing the diversion of NCCs into the subregion adjacent to r3 (marked by the arrowhead [0, 2 h] and dotted box [4 h]) in comparison to the migratory front (asterisk) ( $n$  was at least 12 embryos/experiment). H, Control vs. Trail10B and/or Trail11B morpholino knockdown showing the NCC-free zone adjacent to r3 outlined by a dotted box and diversion of NCCs into this subregion. I, Triple combination knockdown of Colec12/Trail10B/Trail11B with the subregion adjacent to r3 outlined by the dotted box and showing extensive invasion of HNK1-labeled NCCs and diversion from the targets ba1 and ba2. J, K, Measurements of diverted NCCs into the subregion adjacent to r3 in (J) Trail10B and (K) triple combination knockdown. The scalebars are 50  $\mu\text{m}$  in all images.

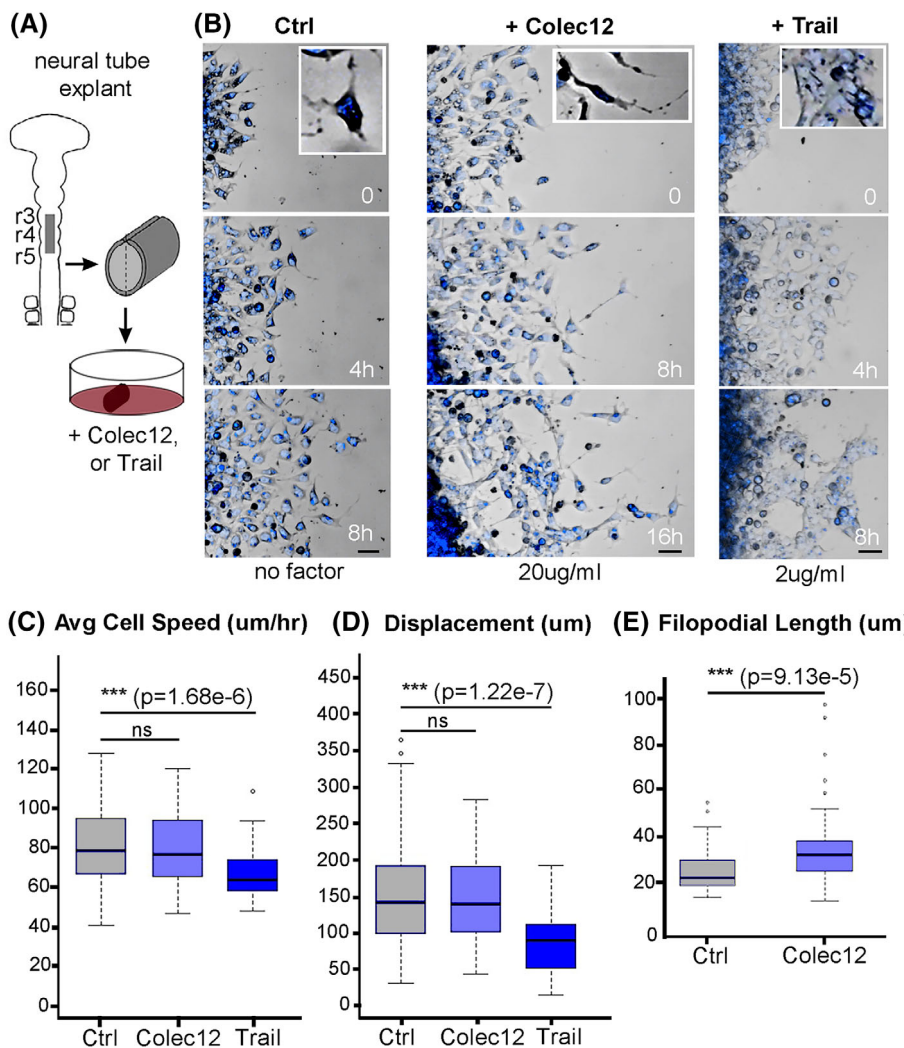


**FIGURE 5** Coculture of NCCs with Colec12 or Trail protein in the media significantly affects NCC morphology and migratory characteristics. **A**, Schematic of cranial neural tube explant culture with Colec12 or Trail protein added to the culture media. **B**, Static images of changes in migrating NCC morphologies extracted from typical time-lapse imaging sessions with insets showing individual NCCs (16 h each, n = 3 neural tube explant cultures for each experiment and >180 cells tracked and analyzed in each experiment). **C**, **D**, Changes in NCC migratory characteristics measured for average cell speed and displacement. **E**, Filopodial length measurements from coculture with Colec12 protein experiments. The scalebars are 20 μm in each image in (B).

and displacement in the presence of Colec12 protein were unchanged (Figure 5C,D).

In striking contrast, when cranial NCCs were exposed to Trail protein in the culture media, NCCs appeared to adhere to one another and move as cell clusters rather than individual cells (Figure 5B; compare Ctrl vs. +Trail images, compare also Movies S2 and S4). Cell speed and displacement were significantly reduced (Figure 5C,D); filopodial lengths were unchanged (data not shown). Closer observation of individual cells revealed changes in cell morphology to resemble a more-rounded phenotype and amoeboid-like motility prior to clustered migration (Figure S1E). This phenotype was consistent with observations in the *in vitro* Trail protein stripe experiments (see Figure 2); the rounded-up cell morphology was more apparent in the presence of Trail protein in comparison to Colec12 and control media (Figure S1F,G). In all culture experiments with any of the aforementioned factors, there was no change in cell directionality (data not shown). Thus, cranial NCC dynamic behaviors are dramatically affected by the presence of Colec12 or Trail in

the culture media and the distinct changes in cell morphology and migratory characteristics suggest signaling through separate downstream pathways.

### 3 | DISCUSSION

We have identified and tested the function of two previously undescribed embryonic neural crest microenvironmental factors, Colec12 and Trail to confine chick cranial NCC trajectories and promote collective cell migration. Computational model simulations of the interplay between cell chemotaxis and cell communication predicted that changes to the cell confinement boundaries within approximately the first one-third (0–400 μm) of the approximately 1,000–1,200 μm stereotypical cranial NCC proximal-to-distal (*x*-direction) migratory pathway would result in diversion of NCC trajectories along the anterior-to-posterior axis (*y*-direction) and disruption of collective cell migration. In agreement with model predictions, we confirmed enhanced expression of Colec12

and Trail expression within the first one-third of the NCC-free zone adjacent to r3, using multiplexed FISH analysis. Loss-of-function of *Colec12* and/or *Trail* resulted in diversion of NCC trajectories in the  $y$ -direction into the r3 NCC-free zone within the first one-third of the migratory pathway and disrupted collective cell migration. By combining *in vitro* *Colec12* or *Trail* protein stripe and coculture assays with confocal time-lapse microscopy, we observed changes in NCC migratory characteristics, cell morphologies, and filopodial dynamics. Together, these data provide unique insights into the spatial requirements to confine cranial NCC trajectories to discrete streams and cell-microenvironmental interactions that promote collective NCC migration.

Computational model simulations predicted the unexpected result that signals confining cranial NCC trajectories are not required along the entire stereotypical migratory pathway from the dorsal neural tube to the

branchial arches. Such predictions highlight the ability of model simulations to rapidly provide insights into the interplay and balance between cell chemotaxis, cell communication, and inhibitory signals to drive collective NCC migration. Our previous modeling efforts had determined the conditions under which a leader NCC responds to a gradient of VEGF chemical signal and invades a 2D domain growing uniformly in time.<sup>24,25</sup> This provided a foundation to examine leader-to-follower cell communication in more detail to be either by leader-to-follower contact (promoting stream migration) or indirectly by NCCs following the path forged by a leader.<sup>40</sup> In this study, we were able to examine how relaxation of the 2D migratory domain boundaries along the anterior-to-posterior axis ( $y$ -direction) affected collective NCC migration along the proximal-to-distal axis ( $x$ -direction) (Figures 1 and 6). For computational convenience, we imposed zero flux boundary conditions at the internal

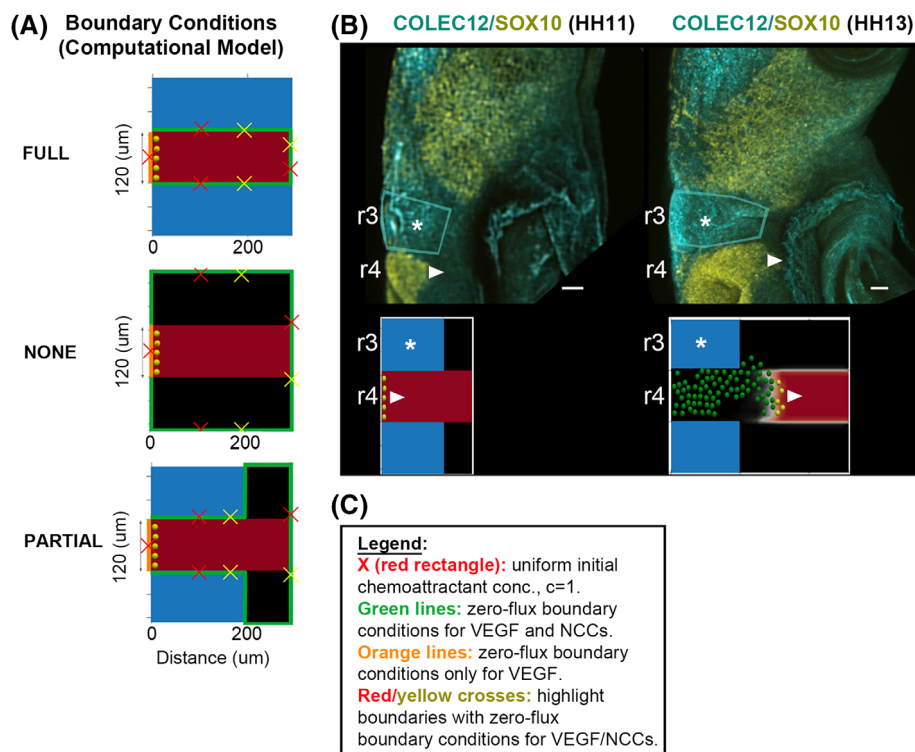


**FIGURE 6** Boundary conditions for the computational model and relationship to *Colec12* expression. A, Different confinement possibilities for the initial set up: (far left) full internal confinement; (middle) no internal confinement; (right) partial internal confinement. The red rectangle corresponds to the region with uniform initial chemoattractant concentration,  $c=1$ . The green wide lines correspond to zero flux boundary conditions for VEGF and NCCs. The orange wide lines correspond to zero flux boundary conditions only for VEGF. Red and yellow crosses highlight boundaries with zero flux boundary conditions for VEGF and NCCs, respectively. On the left the chemoattractant concentration in the black region is zero,  $c=0$ . The blue rectangles represent internal confinement, as before. Yellow circles represent NCCs. B, Comparison of the experimental data of *Colec12/Sox10* expression in HH11 and HH13 embryos (same images as shown in Figure 2A, rotated slightly counter-clockwise) with the *Colec12* expression in the presumptive NCC-free zone adjacent to r3 surrounded by a light blue highlighted line (with asterisk in center) and front of r4 NCC migratory stream (arrowhead), corresponding to the model confinement of NCCs adjacent to the rostral border of the NCC migratory domain at time  $t=0$  and  $t=9$  h of simulation time (marked by an asterisk) and simulated representation of NCCs (leader in yellow and followers in green; front marked by arrow). C, Legend for (A). The scalebars are (B) 50  $\mu\text{m}$ .

boundary for VEGF but this, as we already have zero flux for cells at the boundary, did not significantly affect the qualitative outcome of our key model prediction. Namely, that full model confinement is not necessary for invasion of the branchial arches. Since otic vesicle formation occurs in the subregion adjacent to r5 during cranial NCC migration, it is experimentally challenging to validate the model prediction along the caudal border of the r4 migratory stream, but reasonable along the rostral r3/r4 boundary as performed in this study. To test this, the 2D model may be deployed to analyze trunk NCC migration, where NCCs are confined to discrete streams through neighboring caudal somite halves that offer access to molecular and surgical manipulation. Future modeling efforts may also explore how tissue-based expansion of the chick head mesoderm, recently shown to be heterogeneous in space and time<sup>41</sup> affects the expansion of *Colec12* and *Trail* expression domains and this relationship to discrete NCC migratory streams.

Our expression analysis and in vitro protein stripe data support an inhibitory role for *Colec12* and *Trail* that may be mined for insights into how changes in dynamic cell behaviors promote collective NCC migration. Our integrated RNAscope, immunohistochemistry, and tissue clearing approach allowed us to visualize and confirm the spatial restriction of *Colec12* and *Trail* expression to the subregion lateral to the hindbrain at the axial level of r3, a typical NCC-free zone, with respect to the position of Sox-10 labeled migrating NCCs (Figure 2). Furthermore, we find that *Colec12* protein is expressed adjacent to r3 and r4, and in the tissue along the rostral border of the r4 NCC migratory stream (Figure S1A). This provided motivation to pursue in vitro protein stripe experiments that confirmed the restriction of uncontrolled NCC migration (Figure 2). NCCs were confined to migrate in a very directed manner between *Colec12* and *Trail* protein stripes (Figure 2) with cell morphologies aligned parallel to the protein stripes (Figure 2). NCCs were more confined between the *Colec12* or *Trail* protein stripes the further cells migrated away from the neural tube explant (Figure 2D,F). Knockdown of *Colec12* led to changes in the morphology of r4 NCCs immediately adjacent to the neighboring NCC-free zone adjacent to r3; NCCs displayed enhanced protrusions in the rostral direction (Figure 4) perpendicular to the direction of the target, ba2 (Figure 4).

We observed *distinct* changes in NCC migratory characteristics and morphology depending on coculture with either *Colec12* or *Trail*, suggesting that NCCs use different signaling pathways in response to encountering these factors in the chick head mesoderm (Figure 5). We were surprised to find that coculture with *Colec12* protein led to protracted filopodia, since we were expecting NCCs to

collapse cell protrusions in its presence. However, this observation may represent its function to inhibit rather than repel cell movements (Figure 5). We speculate that lengthened cell protrusions may provide a means for wayward NCCs in the anterior-to-posterior axis (*y*-direction) to recontact cells moving along the proximal-to-distal stereotypical migratory pathway (*x*-direction). In support of this, we have previously observed in vivo NCCs rejoining a neighboring stream after migrating into cranial NCC-free zones<sup>42</sup> and an inability to retract filopodial protrusions after blocking RhoA.<sup>43</sup> Future experiments may shed light on the signals downstream of *Colec12* and *Trail* that regulate cell cytoskeletal properties.

In contrast to our *Colec12* observations and the typical NCC migratory behavior as individuals, we observed NCCs adhering to one another and cluster migration in the presence of *Trail* protein (Figure 5). This resulted in decreased average cell speed and displacement (Figure 5). These features were observed in vivo in the *Colec12/Trail* double knockdown, as invasive NCCs formed discrete linear stream-like arrays of connected cells between the ba1/ba2 streams (Figure 4). These stream-like arrays have previously been observed in mice carrying null mutations for either *Npn2* (*neuropilin2*) or *Sema3F* and typically within the first 200  $\mu\text{m}$  of the NCC migratory pathway.<sup>16</sup> The close proximity of these stream-like arrays in mice and not further downstream may be as a result of *Sema3F* expression in the hindbrain (r3 and r5) rather than paraxial mesoderm. In the presence of *Trail* protein in the culture media, we also observed several NCCs to adopt a rounded phenotype, but continue to move in an amoeboid-like manner (Figure S1E–G; see also Movie S4). Together, these quantitative data may now be integrated into our modeling framework to predict how changes in NCC migratory characteristics and cell morphology may influence collective NCC migration.

The receptors for *COLEC12* are currently unknown. Future mass spectrometry experiments may help to determine candidates whose expression may then be verified in vivo on migrating cranial NCCs and provide a foundation for loss-of-function studies. *COLEC12* has also previously been shown to have high binding specificity for glycans containing a terminal Lewis-X structure.<sup>44</sup> It will be interesting to determine whether Lewis-X is expressed in a similar spatial location as *Colec12*, adjacent to r3 in chick. Further investigation of the role of Lewis-X in *Colec12*-mediated inhibition of NCC migration may include preincubated *Colec12* with Lewis-X before preparing the protein stripe assays and a repeat of the experiments with *Colec12* protein stripes described above, including addition of Lewis-X antibodies (C3D-1 and HI98) into the culture media that have previously been

shown to block its function.<sup>45</sup> This would allow the evaluation of whether inhibitory effects of Colec12 are enhanced by Lewis-X. Together, these data would demonstrate the potential for investigation of signals downstream of Colec12 that may regulate NCC migratory behaviors.

The above findings may have important implications for human neural crest-derived cancers and other aggressive cell phenomena. Interest in TRAIL gained momentum after the observation that TRAIL could selectively kill cancer cells but not normal cells (reviewed by Kimberley et al<sup>46</sup>). This was based on the expression of decoy receptors that could sequester Trail and divert it away from death receptors initially found to be restricted to normal cells.<sup>35</sup> However, the presence or absence of decoy receptors may be an unreliable indicator of sensitivity, and in some tumors Trail expression has been implicated as an immune evasion mechanism.<sup>47</sup> In treatment of melanoma, emerging therapeutic strategies are combining known clinically approved kinase inhibitors with TRAIL-induced apoptosis, using second generation TRAIL receptor agonists.<sup>29</sup> However, TRAIL resistance in metastatic melanoma remains a problem.<sup>48</sup> Future studies that examine the downstream signals in embryonic NCCs that escape TRAIL-induced apoptosis may shed light on the interplay of downstream signals that prevent the activation of *Caspase-3* as a no return step in apoptosis and inform the design of synthetic TRAIL receptor agonists. Furthermore, since human metastatic melanoma cell lines may be readily transplanted onto the vascularized chick chorioallantoic membrane (CAM)<sup>49</sup> or into the chick embryonic NCC microenvironment,<sup>50,51</sup> these in vivo models may offer a more rapid means than typical xenografts to test the efficiency of emerging TRAIL sensitizing agents. Also, COLEC12 has been studied in the innate immune system and implicated in brain development and muscular dystrophy, respectively.<sup>52</sup> However, its functional role in cancer remains largely unexplored.<sup>53</sup> Identification of the receptor(s) for Colec12 ligand and the study of the role of Lewis-X mentioned above may provide the foundation to investigate the potential for COLEC12 to mitigate human neural crest-derived cancer cell invasion.

## 4 | EXPERIMENTAL PROCEDURES

### 4.1 | Computational model

In the computational model, we assume that there are two types of cells, namely, “leaders” and “followers”, with a fixed number of leader cells. The leaders undertake a biased random walk with volume exclusion up a

cell-induced gradient of chemoattractant. We use a reaction-diffusion equation to model the dynamics of the chemoattractant VEGF. The leaders perform this biased random walk by extending three filopodia in random directions per time step. These filopodia can sense the concentration of chemoattractant at their tip, and the cell moves in the direction of the highest concentration sensed, provided it is higher by a threshold value than that at the position of the center of the cell. If there is no measured difference, then the cell moves in a random direction. On the other hand, followers are either in a stream, tunnel or move randomly. A stream consists of a group of followers that are close to each other with at least one of the cells close to a leader. All the followers in a stream move in the same direction as the leader that is at the front of the stream. If a follower is close to more than one leader, so that it may be part of more than one stream, then the cell randomly chooses which leader to follow. The tunneling mechanism, which approximates the extracellular matrix degradation induced by the leader cells,<sup>40</sup> is modeled by recording the history of leader positions, which we define as a “tunnel”. If a follower is sufficiently close to a tunnel, then it starts moving along that tunnel toward the front of the stream. We include a simplified version of phenotype switching between leaders and followers based on the position of a cell within a migratory stream.

We assumed a 2D rectangular growing domain to describe the region between the neural tube and the branchial arches. We assumed that the growth of the domain is uniform in space and logistic in time. The boundary conditions are modeled as follows (Figure 6E): new cells enter the domain at a constant rate at the left-hand (proximal) boundary (the neural tube). There is an attempt to insert a new cell at every time step with a center at a random position along the  $y$ -axis with the coordinate “ $x = \text{cell radius}$ ”, but volume exclusion impedes constant influx, that is a new cell may not be inserted if by entering the domain it will overlap with another cell which is already in the domain. The influx of NCCs is only allowed at the left-hand boundary of the rectangular domain, while zero flux boundary conditions for cells are set at the other three boundaries of the rectangular domain. Zero flux boundary conditions for the cells are defined as follows: a cell cannot move outside the domain but it may extend its filopodia outside the domain. If a subset of its filopodia are extended outside the domain, then the direction of cell movement is determined by the filopodia inside the domain. If all of its filopodia are extended outside the domain, then the cell does not move. We assume zero flux boundary conditions everywhere for the chemoattractant. When the extent of the internal confinement boundary assumption is relaxed,

the boundary conditions are applied to a larger domain specified by the confinement restrictions.

To investigate the effect of the proximal-to-distal length of an internal confinement boundary we defined the following different cases: a full internal confinement boundary, no internal confinement and a partial internal confinement boundary (of varying proximal-to-distal length). In the full internal confinement case, the migratory domain is defined as a rectangular domain of width 120  $\mu\text{m}$  with the zero flux boundary conditions for chemoattractant and NCCs imposed along the top and bottom bounding edges, *ceteris paribus* (Figures 1A and 6E). This domain corresponds to the migratory domain previously used in the models of chick NCC migration.<sup>24-26</sup> To model the case with no internal confinement, we simply use a domain of width 360  $\mu\text{m}$  with zero flux boundary conditions for chemoattractant and NCCs imposed along the top and bottom bounding edges (Figure 1B). In the partial internal confinement case, part of the domain is modeled as in the full internal confinement case, and part of the domain as in the no internal confinement case (Figure 1F). In the no internal confinement case, we still assume that the cells only enter the domain in a confined region (width 120  $\mu\text{m}$ ). We assume that the length of the internal confinement boundary does not elongate as the domain grows. We fix the value of the confinement boundary length. This assumption is used to clearly distinguish the effect of a fixed internal confinement boundary length but in reality, the internal confinement boundary could be elongating as the domain grows and, in that scenario, the fraction of the confined domain may not remain constant, due to our previous observation domain growth is spatially non-uniform.<sup>41</sup> Boundary conditions for the chemoattractant (VEGF), NCCs, and internal confinement are shown in Figure 6E.

## 4.2 | Embryos

Fertilized White Leghorn chicken eggs (Centurion Poultry, Inc., Lexington, GA) were incubated in a humidified incubator at 38°C to the desired developmental stage (HH).<sup>34</sup>

## 4.3 | Identification of *Colec12* and *Trail* in the chick embryonic neural crest microenvironment

As previously described in McLennan et al.<sup>26</sup> a microarray screen was performed to identify genes enriched in the NCC exclusion zone adjacent to r3. Briefly, at stages HH11, HH13, and HH15, tissue was isolated in triplicate

from the subregion adjacent to r3 and from leader NCCs from the r4 migratory stream and then analyzed by microarray analysis. Model simulations helped to guide us to compare gene expression in the two sets of samples and generate a short list of candidate genes with elevated expression in the subregion adjacent to r3.

## 4.4 | Multiplexed FISH by RNAscope

RNAscope on whole chick embryos was performed as previously described.<sup>30</sup> Briefly, embryos were harvested and fixed in 4% paraformaldehyde for 2 h at room temperature. Following a dehydration gradient in methanol, embryos were stored overnight at  $-20^{\circ}\text{C}$ . After rehydration, embryos were digested in diluted protease solution from Advanced Cell Diagnostics (Newark, CA). Sox10, *Colec12*, and *Trail* RNAscope probes were designed by Advanced Cell Diagnostics against GenBank accession numbers NM\_204792, NM\_001039599, and NM\_204379, respectively. Probes were hybridized with embryos overnight at 40°C and were amplified and labeled the following day. The embryos were then optically cleared by the FRUIT method<sup>54</sup> prior to imaging. Probes were ordered from IDT (Coralville, IA), pooled, and extended as described by Kishi et al.<sup>55</sup> Embryos were harvested, fixed, dehydrated in methanol, and rehydrated as described above for RNAscope. Embryos were then incubated in 5  $\mu\text{g}/\text{mL}$  proteinase K (V3021; Promega, Madison, WI) in PBST (PBS + 0.1% Tween-20) for 5 min at room temperature. Embryos were washed three times with PBST, then twice with hybridization wash buffer (2 $\times$  SSC, 1% Tween-20, 40% formamide). Extended probes were diluted in hybridization buffer (2 $\times$  SSC, 1% Tween-20, 40% formamide, 10% dextran sulfate), 2  $\mu\text{g}$  in 200  $\mu\text{L}$  total volume, and hybridized with embryos overnight at 43°C. Embryos were washed three times with hybridization wash buffer at 43°C, washed twice with 2 $\times$  SSC + 0.1% Tween-20 at 43°C, then returned to room temperature and washed twice with PBST. Complementary imager probes ordered from IDT were diluted to 0.2  $\mu\text{M}$  in 200  $\mu\text{L}$  hybridization buffer (1 $\times$  PBS, 0.2% Tween-20, 10% dextran sulfate) and hybridized with embryos at 37°C for 30 min. Embryos were washed three times with PBST at 37°C, then returned to room temperature for imaging.

## 4.5 | In vitro NCC assays

Stripe assays using cranial neural tubes (r3-r5) were performed as previously described.<sup>56</sup> Stripe assays were generally performed using 40  $\mu\text{m}$  stripe matrices (Karlsruher

Inst Fur Technologie, Karlsruhe, Germany). In order to visualize the stripes, Texas Red-BSA (A23017, Thermo Fisher Scientific, Waltham, MA) was added to all stripe solutions at 20  $\mu\text{g}/\text{mL}$ . Control stripes contained no added protein. Experimental stripes contained recombinant human Colec12 or Trail proteins (2690-CL-050, 375-TL-010; R&D Systems, Minneapolis, MN) at the concentrations listed in the results section of this paper. Cranial neural tubes were adhered to the prepared stripe assay plates and incubated in 5  $\mu\text{g}/\text{mL}$  Hoechst in media for 5 min, which was then removed and replaced with fresh media. The plates were transferred to an LSM 800 (Zeiss, Oberkochen, Germany) with an incubator box set to 37°C. After at least 1 h of equilibration time, the neural tubes and surrounding area were imaged overnight in 5-min time intervals. Cells were automatically detected using spot detection in Imaris (Bitplane) and counted at the 12 h time point as on or off stripes and normalized to stripe area as calculated by Imaris. *P* values were calculated using a standard Student's *t*-test. Data distribution was assumed to be normal, but this was not formally tested. The number of explanted neural tubes analyzed were (negative Ctrl = 5, Colec12 = 4, Trail = 6) and the number of cells counted were (Ctrl = 629, Colec12 = 349, Trail = 428). For neural crest cultures with protein added to the media, cranial neural tubes (r3-r5) were isolated and cultured as previously described.<sup>7</sup> Colec12 or Trail protein was added to media at 20 or 2  $\mu\text{g}/\text{mL}$ , respectively. Cultures were imaged as described above for neural crest stripe assays. Cells were automatically detected and tracked using spot detection in Imaris, which generated speed and straightness calculations for each track. *P* values were calculated using a standard Student's *t*-test.

#### 4.6 | In vivo perturbations

All morpholinos were designed and synthesized by Gene Tools, LLC (Philomath, OR). Electroporations of morpholino into the dorsal neural tube were performed as previously described.<sup>57</sup> To electroporate morpholino into the paraxial mesoderm, fluorescein-labeled morpholino was first combined with a carrier plasmid (pMES-h2b-mCherry) at 1:1 ratio, giving a morpholino concentration of 0.5 mM and carrier concentration of 2.5  $\mu\text{g}/\mu\text{L}$ . The morpholino/carrier mixture was injected at multiple sites in the mesoderm on one side of the neural tube near the hindbrain in HH9 embryos, and electrodes were placed above and below injections for electroporation. After electroporation, sterile Ringer's solution was pipetted onto the embryo, and the opening in the eggshell was sealed with tape. For overexpression experiments,

Colec12 or Trail protein was microinjected into the mesoderm adjacent to r4 at a concentration of 500  $\mu\text{g}/\text{mL}$  and volume of approximately 2–4 pL. Eggs were then reincubated for 16 h, harvested, and fixed in 4% paraformaldehyde at room temperature for 2 h. Embryos (at least  $n = 12$  for each experiment) were then processed for HNK1 staining to visualize migrating NCCs. Morpholinos were either injected and electroporated with DiI before being reincubated for 12 h or injected and electroporated without DiI before being reincubated for 16 h. Time-lapse imaging was performed as previously described by McKinney et al.<sup>58</sup>

#### 4.7 | Image analysis and measurement of projected area of NCC migration

We calculated the projected area covered using the “Surfaces” function of Imaris (Bitplane) to create a surface mask. We then calculated the area of the fluorescence signal (HNK1) using the masked arch surface. We set a consistent intensity threshold to the same value for each data set, a surface grain size of 1  $\mu\text{m}$  was set, the diameter of the largest sphere was set to 1  $\mu\text{m}$ , and then the automatic “Surfaces” function was applied. The box plots were generated by using the values from each data set indicated. X indicates outliers, and the box plots and whiskers indicate the quartiles and range, respectively, of each data set. *P* values were calculated using a standard Student's *t*-test or paired *t*-test. Data distribution was assumed to be normal, but this was not formally tested.

#### 4.8 | Time-lapse imaging of whole chick embryos on EC culture

Live embryos for time-lapse imaging were mounted on EC culture dorsal-side down beginning at HH9 or HH10 modifying the protocols,<sup>58,59</sup> such that the EC culture was plated with only 500  $\mu\text{L}$  of liquid to reduce light scattering. Confocal z-stacks were collected every 5 min for up to 12 h with a 10 $\times$  0.45 objective.

#### 4.9 | Immunostaining

Immunohistochemistry was performed on fixed whole embryos or heads only by first permeabilizing in PBS + 0.5% Triton X-100 at room temperature for 1 h. Embryos were incubated in blocking buffer (PBS + 0.1% Triton X-100 + 4% BSA) for 2–4 h at room temperature, then incubated in primary antibody diluted in blocking buffer overnight at 4°C. Embryos were washed three

times in blocking buffer for >1 h per wash at 4°C, then incubated in secondary antibody diluted in blocking buffer overnight at 4°C. Embryos were washed three times in PBS for >1 h per wash at 4°C, then either kept whole or bisected down the midline as described previously and mounted in PBS for imaging.

### AUTHOR CONTRIBUTIONS

**Rebecca McLennan:** Conceptualization (equal); data curation (equal); formal analysis (equal); funding acquisition (equal); methodology (equal); visualization (equal); writing – original draft (equal); writing – review and editing (supporting). **Rasa Giniunaite:** Data curation (equal); formal analysis (equal); methodology (equal); software (equal); writing – original draft (equal); writing – review and editing (supporting). **Katie Hildebrand:** Data curation (supporting); formal analysis (supporting); investigation (supporting); methodology (equal); validation (equal); visualization (supporting); writing – original draft (supporting); writing – review and editing (supporting). **Jessica M. Teddy:** Data curation (supporting); methodology (supporting); software (supporting). **Jennifer C. Kasemeier-Kulesa:** Data curation (supporting); formal analysis (supporting); methodology (supporting); writing – review and editing (supporting). **Lizbeth Bolanos:** Data curation (supporting); methodology (supporting); visualization (supporting). **Ruth E. Baker:** Conceptualization (supporting); investigation (supporting); software (supporting); supervision (supporting); writing – original draft (supporting). **Philip K. Maini:** Conceptualization (supporting); investigation (supporting); project administration (supporting); software (supporting); supervision (equal); writing – original draft (equal); writing – review and editing (supporting). **Paul M. Kulesa:** Conceptualization (equal); data curation (equal); funding acquisition (equal); investigation (equal); project administration (lead); supervision (lead); writing – original draft (equal); writing – review and editing (lead).

### ACKNOWLEDGMENTS

P.M.K. would like to acknowledge the kind and generous funding from the National Institutes of Health/NICHHD and the Stowers Institute for Medical Research. The authors thank members of the Stowers Institute Microscopy, Histology, and Molecular Biology core facilities.

### ORCID

Paul M. Kulesa  <https://orcid.org/0000-0001-6354-9904>

### REFERENCES

1. Le Douarin NM, Kalcheim C. *The Neural Crest*. 2nd ed. New York: Cambridge University Press; 1999.
2. Vega-Lopez GA, Cerrizuela S, Tribulo C, Aybar MJ. Neurocris-topathies: new insights 150 years after the neural crest discovery. *Dev Biol*. 2018;444:S110-S143.
3. Siismets EM, Hatch NE. Cranial neural crest cells and their role in the pathogenesis of craniofacial anomalies and coronal craniosynostosis. *J Dev Biol*. 2020;8(3):18.
4. Cerrizuela S, Vega-Lopez GA, Aybar MJ. The role of teratogens in neural crest development. *Birth Defects Res*. 2020;112(8):584-632.
5. Ibarra BA, Atit R. What do animal models teach us about congenital craniofacial defects? *Adv Exp Med Biol*. 2020;1236:137-155.
6. Liu JA, Cheung M. Neural crest stem cells and their potential therapeutic applications. *Dev Biol*. 2016;19(2):199-216.
7. McLennan R, Teddy JM, Kasemeier-Kulesa JC, Romine MH, Kulesa PM. Vascular endothelial growth factor (VEGF) regulates cranial neural crest migration in vivo. *Dev Biol*. 2010;339(1):114-125.
8. Kasemeier-Kulesa JC, McLennan R, Romine MH, Kulesa PM, Lefcort F. CXCR4 controls ventral migration of sympathetic precursor cells. *J Neurosci*. 2010;30(39):13078-13088.
9. Olesnick-Killian EC, Birkholz DA, Artinger KB. A role for chemokine signaling in neural crest cell migration and craniofacial development. *Dev Biol*. 2009;333(1):161-172.
10. Theveneau E, Steventon B, Scarpa E, et al. Chase-and-run between adjacent cell populations promotes directional collective migration. *Nat Cell Biol*. 2013;15(7):763-772.
11. Trainor PA, Krumlauf R. Patterning the cranial neural crest: hindbrain segmentation and *hox* gene plasticity. *Nat Rev Neurosci*. 2000;1(2):116-124.
12. Trainor PA, Sobieszczuk D, Wilkinson D, Krumlauf R. Signaling between the hindbrain and paraxial tissues dictates neural crest migration pathways. *Development*. 2002;129(2):433-442.
13. Kulesa PM, Ellies DL, Trainor PA. Comparative analysis of neural crest cell death, migration, and function during vertebrate embryogenesis. *Dev Dyn*. 2004;229:14-29.
14. Golding JP, Trainor P, Krumlauf R, Gassman M. Defects in pathfinding by cranial neural crest cells in mice lacking the neuregulin receptor ErbB4. *Nat Cell Biol*. 2000;2(2):103-109.
15. Osborne NJ, Begbie J, Chilton JK, Schmidt H, Eickholt BJ. Semaphorin/neuropilin signaling influences the positioning of migratory neural crest cells within the hindbrain region of the chick. *Dev Dyn*. 2005;232(4):939-949.
16. Gammill LS, Gonzalez C, Gu C, Bronner-Fraser M. Guidance of trunk neural crest migration requires neuropilin 2/-semaphorin 3F signaling. *Development*. 2006;133(1):99-106.
17. Smith A, Robinson V, Patel K, Wilkinson DG. The EphA4 and EphB1 receptor tyrosine kinases and ephrin-B2 ligand regulate targeted migration of branchial neural crest cells. *Curr Biol*. 1997;7(8):561-570.
18. Szabo A, Melchionda M, Nastasi G, et al. In vivo confinements promotes collective migration of neural crest cells. *J Cell Biol*. 2016;213(5):543-555.
19. Mellott DO, Burke RD. Divergent roles for Eph and ephrin in avian cranial neural crest. *BMC Dev Biol*. 2008;8:56.
20. Merchant B, Edelstein-Keshet L, Feng JJ. A Rho-GTPase based model explains spontaneous collective migration of neural crest cell clusters. *Dev Biol*. 2018;444:S262-S273.
21. Merchant B, Feng JJ. A Rho-GTPase based model explains group advantage in collective chemotaxis of neural crest cells. *Phys Biol*. 2020;17(3):036002.



22. Szabo A, Theveneau E, Turan M, Mayor R. Neural crest streaming as an emergent property of tissue interactions during morphogenesis. *PLoS Comp Biol*. 2019;15(4):e1007002.
23. Woods ML, Carmona-Fontaine C, Barnes CP, Couzin ID, Mayor R, Page KM. Directional collective cell migration emerges as a property of cell interactions. *PLoS One*. 2014;9(9):e104969.
24. McLennan R, Dyson L, Prather KW, et al. Multiscale mechanisms of cell migration during development: theory and experiment. *Development*. 2012;139(16):2935-2944.
25. McLennan R, Schumacher LJ, Morrison JA, et al. Neural crest migration is driven by a few trailblazer cells with a unique molecular signature narrowly confined to the invasive front. *Development*. 2015;142(11):2014-2025.
26. McLennan R, Bailey CM, Schumacher LJ, et al. DAN (NBL1) promotes collective neural crest cell migration by restraining uncontrolled invasion. *J Cell Biol*. 2017;216(10):3339-3354.
27. Schumacher L, Kulesa PM, McLennan R, Baker RE, Maini PK. Multidisciplinary approaches to understanding collective cell migration in developmental biology. *Open Biol*. 2016;6:160056.
28. Ma YJ, Hein E, Munthe-Fog L, et al. Soluble collectin-12 (CL-12) is a pattern recognition molecule initiating complement activation via the alternative pathway. *J Immunol*. 2015;195(7):3365-3373.
29. Fleten KG, Florenes VA, Prasmickaite L, et al. hvTRA, a novel TRAIL receptor agonist, induces apoptosis and sustained growth retardation in melanoma. *Cell Death Discov*. 2016;2:16081.
30. Morrison JA, McKinney MC, Kulesa PM. Resolving in vivo gene expression during collective cell migration using an integrated RNAscope, immunohistochemistry, and tissue clearing method. *Mech Dev*. 2017;148:100-106.
31. Fukuda M, Ohtani K, Jang SJ, et al. Molecular cloning and functional analysis of scavenger receptor zebrafish CL-P1. *Biochim Biophys Acta*. 2011;1810(2):1150-1159.
32. Micheau O, Shirley S, Dufour F. Death receptors as targets in cancer. *Br J Pharmacol*. 2013;169(8):1723-1744.
33. Snajdauf M, Havlova K, Vachtenheim J, et al. The TRAIL in the treatment of human cancer: an update on clinical trials. *Front Mol Biosci*. 2021;8:628332.
34. Hamburger V, Hamilton HL. A series of normal stages in the development of the chick embryo. *J Morphol*. 1951;88(1):49-92.
35. Pan G, O'Rourke K, Chinnaiyan AM, et al. The receptor for the cytotoxic ligand TRAIL. *Science*. 1997;276:111-113.
36. Walczak H, Degli-Esposti MA, Johnson RS, et al. TRAIL-R2: a novel apoptosis-mediating receptor for TRAIL. *EMBO J*. 1997;16:5386-5397.
37. MacFarlane M, Ahmad M, Srinivasula SM, Fernandes-Alnemri T, Cohen GM, Alnemri ES. Identification and molecular cloning of two novel receptors for the cytotoxic ligand TRAIL. *J Biol Chem*. 1997;272:25417-25420.
38. Emery JG, McDonnell P, Burke MB, et al. Osteoprotegerin is a receptor for the cytotoxic ligand TRAIL. *J Biol Chem*. 1998;273:14363-14367.
39. Morrison JA, McLennan R, Wolfe JA, et al. Single-cell transcriptome analysis of avian neural crest migration reveals signatures of invasion and molecular transitions. *Elife*. 2017;6:e28415.
40. McLennan R, McKinney MC, Teddy JM, et al. Neural crest cells bulldoze through the microenvironment using Aquaporin 1 to stabilize filopodia. *Development*. 2020;147(1):dev185231.
41. McKinney MC, McLennan R, Giniunaite R, et al. Visualizing mesoderm and neural crest cell dynamics during chick head morphogenesis. *Dev Biol*. 2020;461(2):184-196.
42. Kulesa PM, Fraser SE. Neural crest cell dynamics revealed by time-lapse video microscopy of whole chick embryo explant cultures. *Dev Biol*. 1998;204(2):327-344.
43. Rupp PA, Kulesa PM. A role for RhoA in the two-phase migratory pattern of post-otic neural crest cells. *Dev Biol*. 2007;311(1):159-171.
44. Coombs PJ, Graham SA, Drickamer K, Taylor ME. Selective binding of the scavenger receptor C-type lectin to Lewis<sup>x</sup> trisaccharide and related glycan ligands. *J Biol Chem*. 2005;280(24):22993-22999.
45. Brazil JC, Sumagin R, Cummings RD, Louis NA, Parkos CA. Targeting of neutrophil Lewis X blocks transepithelial migration and increases phagocytosis and degranulation. *Am J Pathol*. 2016;186(2):297-311.
46. Kimberley FC, Screaton G. Following a TRAIL: update on a ligand and its five receptors. *Cell Res*. 2004;14(5):359-372.
47. Koyama S, Koike N, Adachi S. Expression of TNF-related apoptosis-inducing ligand (TRAIL) and its receptors in gastric carcinoma and tumor-infiltrating lymphocytes: a possible mechanism of immune evasion of the tumor. *J Cancer Res Clin Oncol*. 2002;128(2):73-79.
48. Eberle J. Countering TRAIL resistance in melanoma. *Cancers*. 2019;11:656.
49. Bailey CM, Kulesa PM. Dynamic interactions between cancer cells and the embryonic microenvironment regulate cell invasion and reveal EphB6 as a metastasis suppressor. *Mol Cancer Res*. 2014;12(9):1303-1313.
50. Kulesa PM, Kasemeier-Kulesa JC, Teddy JM, et al. Reprogramming metastatic melanoma cells to assume a neural crest cell-like phenotype in an embryonic microenvironment. *Proc Natl Acad Sci U S A*. 2006;103(10):3752-3757.
51. Kasemeier-Kulesa JC, Romine MH, Morrison JA, Bailey CM, Welch DR, Kulesa PM. NGF reprograms metastatic melanoma to a bipotent glial-melanocyte neural crest-like precursor. *Biol Open*. 2018;7(1):bio030817.
52. Ohtani K, Suzuki Y, Eda S, et al. The membrane-type collectin CL-P1 is a scavenger receptor on vascular endothelial cells. *J Biol Chem*. 2001;276(47):44222-44228.
53. Koudelkova P, Costina V, Weber G, et al. Transforming growth factor- $\beta$  drives the transendothelial migration of hepatocellular carcinoma cells. *Int J Mol Sci*. 2017;18(10):2119.
54. Hou B, Zhang D, Zhao S, et al. Scalable and DiI-compatible optical clearance of the mammalian brain. *Front Neuroanat*. 2015;9:19.
55. Kishi JY, Lapan SW, Beliveau B, et al. SABER amplifies FISH: enhanced multiplexed imaging of RNA and DNA in cells and tissues. *Nat Methods*. 2019;16:533-544.
56. Krull CE, Lansford R, Gale NW, et al. Interactions of Eph-related receptors and ligands confer rostrocaudal pattern to trunk neural crest migration. *Curr Biol*. 1997;7(8):571-580.
57. McLennan R, Kulesa PM. In vivo analysis reveals a critical role for neuropilin-1 in cranial neural crest cell migration in chick. *Dev Biol*. 2007;301(1):227-239.
58. McKinney MC, Fukatsu K, Morrison J, McLennan R, Bronner ME, Kulesa PM. Evidence for dynamic rearrangements but lack of fate or position restrictions in premigratory avian trunk neural crest. *Development*. 2013;140(4):820-830.

59. Chapman SC, Collignon J, Schoenwolf GC, Lumsden A. Improved method for chick whole embryo culture using a filter paper carrier. *Dev Dyn*. 2001;220(3):284-289.

### SUPPORTING INFORMATION

Additional supporting information can be found online in the Supporting Information section at the end of this article.

**How to cite this article:** McLennan R, Giniunaite R, Hildebrand K, et al. Colec12 and Trail signaling confine cranial neural crest cell trajectories and promote collective cell migration. *Developmental Dynamics*. 2023;252(5):629-646. doi:[10.1002/dvdy.569](https://doi.org/10.1002/dvdy.569)